CHAPTER 4

DISCUSSION AND CONCLUSION

4.1 Uncertainties in earthquake analysis

In this study, 210 local seismic events in southern Thailand have been analyzed, 173 earthquake event and 37 blasting events. The seismic events are generally described with 1) origin time, 2) location, and 3) the magnitude of the event. However, all each of these parameters come with uncertainties, which depended, for example, on the velocity model used, the regional geology structure, or the data processing with P- and S-wave identification. In the following chapters an attempt is made to identify, characterize and partly semi-quantify these uncertainties in the earthquake analysis.

4.1.1 Different velocity models

In Chapter 1.1.7, three different velocity models are outlined, IASP91-, AK135- and JB-model. The velocity models represent the average crustal and Upper Mantle geology with the related seismic velocities. They comprise subsurface horizontal layers with a certain depth and with seismic velocities (Vp and Vs) assigned for every layer. The three velocity models are quite similar, however small differences exists.

For the IASP91 and AK135 velocity model the first layer has a thickness of 20 km and with same P-wave velocity (5.8 km/s), but with a different S-wave velocity (3.36 km/s and 3.46 km/s, respectively). In the JB velocity model the depth of the first layer it at 15.73 km, and the velocity are Vp = 5.56 km/s and Vs = 3.36 km/s. The second layer in the IASP91 and AK135 velocity models is at 35 km depth, which represents the Moho Discontinuity, or the crust-mantle boundary. The P-wave velocities are the same (6.50 km/s), but there are small differences in the S-wave velocities (3.75 km/s and 3.85 km/s, respectively). For the JB velocity model the depth is at 33.6 km and the velocities are Vp = 6.49 km/s and Vs = 3.74 km/s (see Chapter 1.1.7).

Until now, there is no regional seismic velocity model for Southern Thailand available. Therefore, the JB Velocity Model was used for analyzing local events in Southern Thailand (see Chapter 2.10). As shown above, there are differences between the JB Velocity Model and the two others, the IASP91 and AK135 velocity model. Table 4.1 examines the differences in the earthquake location using the three different velocity models. The distance data were determined from the given distance-traveltime tables for the three different velocity models (see Chapter 1.1.7).

The analysis was done for 0 km depths for two different delta times between the P- and S-wave arrival, at 5 s and at 20 s (see Table 4.1). The shorter delta time would involve only the direct phases (Pg and Sg), whereas the longer delta time would involve the refracted phases (Pn and Sn).

Table 4.1: Comparison of the epicenter distance for different velocity models for earthquakes at 0 km depth. The results for two delta times at 5 s and 20 s are shown.

Δt (s)	**Phase**	**Dist (km)**	**Velocity Model**
5	Pg, Sg	40.28	JB
		39.90	IASP91
		42.83	AK135
20	Pn, Sn	161.15	JB
		154.32	IASP91
		164.07	AK135

Table 4.1 shows that for the same delta time the resulting earthquake distances is different. For Δt=5 s the difference between the JB and the AK135 velocity model is 2.55 km further away, whereas between the JB and the IASP91 the difference is 0.38 km, but closer. At Δt=20 s the differences increase, with 6.83 km closer, comparing JB and IASP91, and 2.92 km further comparing JB and AK135.

Therefore, the velocity model chosen in the earthquake location analysis can have an effect on the location in the order of a few km. This is because of differences in the layer depth and even more important differences in the seismic velocities assigned for each layer.

4.1.2 Seismic phase identification

The JB travel time table comprises of three different phases for local earthquake: Pg and Sg, P* and S*, and Pn and Sn (see Figure 4.1). However, during the analysis of the seismograms the phase identification was difficult. Therefore, only two phases have been identified and its traveltimes used, Pg and Sg, Pn and Sn, as outlined in Chapter 2.10, but not the P* and S*. Instead of using the traveltime for the P*-phase, either the traveltime for Pg or Pn has been used. The same accounts for the S-wave phases. As the JB travel time comprises three phases for each seismic velocity, this process lead to a decrease in the resulting delta time for earthquake in a distance between 112 km and 168 km.

Figure 4.2 shows the increase in delta time if the P* and S* phases would have been identified and used in the subsequent calculations. Between 112 and 143 km the Pg and Pn phases have been used instead of P*, which resulted in a decrease of delta time of maximal 0.6 s. Similar accounts for the S-wave phase, but with a smaller decrease in delta time.

For example, if the delta time would be determined with 16.45 s, and the phases would be P* and Sg the corresponding distance would be 135 km. However, with the same delta time and the phases identified as Pg and Sg, the corresponding distance would be 140 km. As shown in Figure 4.2 this effect is related to the identification of P* and therefore limited for delta times between 13.16 s and 20.70 s, corresponding to 112 km and 168 km if using all three phases.

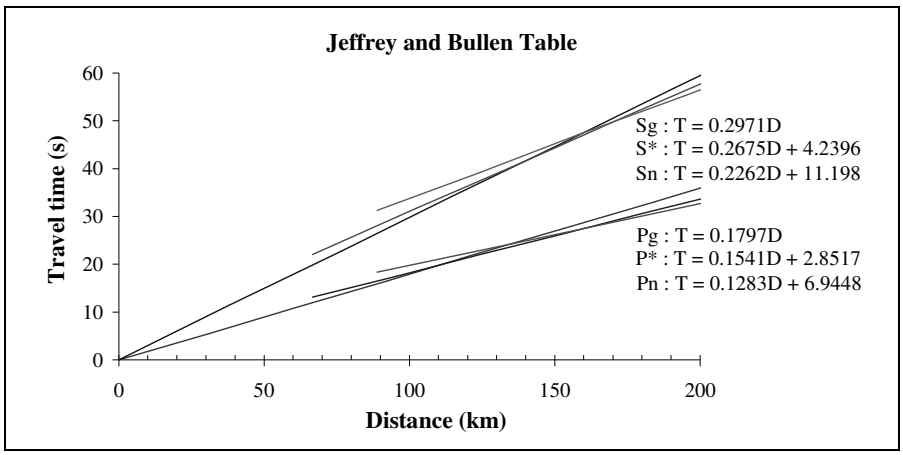

Figure 4.1. Traveltime (T) versus distance (D) for the different phases Pg, P*, Pn, Sg, S* and Sn, based on JB traveltime-distance data (Chapter1.1.7).

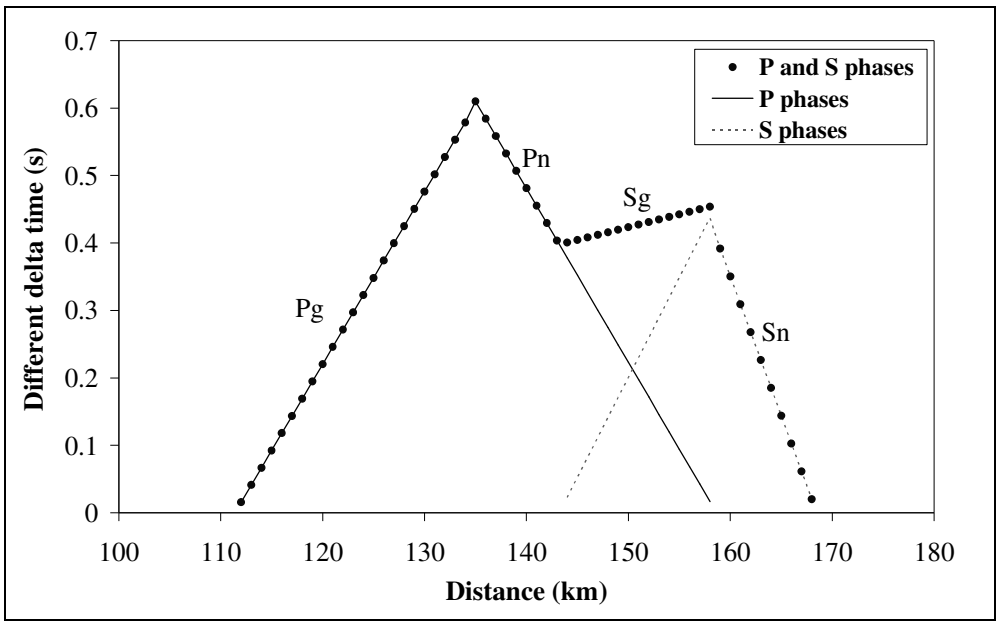

Figure 4.2. The increase in delta time versus distance using all three phases of the JB local earthquake travel time tables instead of only the Pg and Sg, and Pn and Sn phases (without P* and S*). The maximum increase is at 135 km distance and is related to the P phases.

4.1.3 Different earthquake depths

During the earthquake analysis in this study, the JB traveltime tables for local events with 0 km depths were used. However, this might be not realistic for most of the events, except the man made events. Any increase in the hypocenter depth will also have an effect on the epicenter location. The change depends on whether direct seismic waves or refracted seismic waves were recorded at the seismometer.

Using the same delta time between the P- and S-wave arrival, the distance from the epicenter to a seismic station decreases with increasing depth, for the direct Pg- and Sg-phases. For the refracted waves (Pn- and Sn-phases), the epicenter distance increases with increasing depth (see Table 4.2, Figure 4.3 and 4.4).

Table 4.2 shows the linear relationships between delta time and distance for different depth and different phases based on the JB traveltime-distance-depth data, with examples given. The schematic cross sections in Figure 4.3 and 4.4 show the ray paths of the waves for each example.

Table 4.2: Linear relationships between delta time and distance for different depths and phases based on the JB travel time-distance-depth data. Examples at Δt=8.6 s with Pg and Sg phase, and at Δt=22 s with Pn and Sn phase. D=distance in km.

Depth	Pg, Sg Phase		Pn, Sn Phase	
(km)	Equations	D (km)	Equations	D (km)
0	Δt = 0.1172D	73.38	Δt = 0.0981D + 4.1911	181.54
6	Δt = 0.1171D + 0.1911	71.81	Δt = 0.0981D + 3.7845	185.68
15	Δt = 0.1169D + 0.3815	70.30	Δt = 0.0981D + 3.1745	191.90
24			Δt = 0.0981D + 2.6333	197.42
30			Δt = 0.0981D + 2.2724	201.10

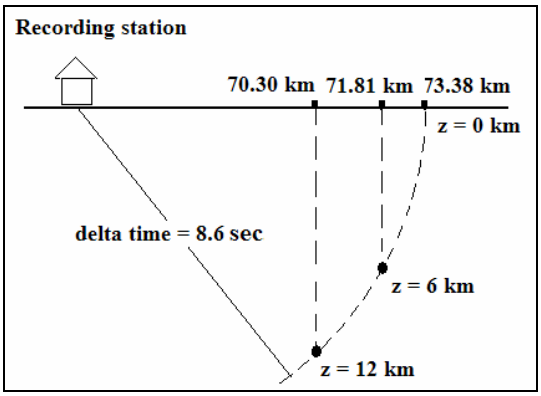

Figure 4.3. Schematic cross section of epicenter distance change for different hypocenter depths, for direct waves (Pg- and Sg-phases) using the same delta time (8.6 s). Data based on JB traveltime-distance-depth data (see Table 4.2).

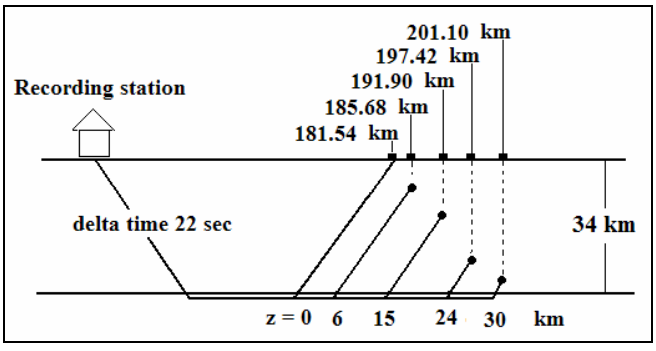

Figure 4.4. Schematic cross section of epicenter distance change for different hypocenter depths, for Pn- and Sn-phases and using the same delta time (22 s). Data based on JB traveltime-distance-depth tables (see also Table 4.2).

In the next step, the effect of increasing hypocenter depth onto the epicenter distance for different delta time values was examined, as shown in Table 4.3. For the direct waves, examples at 1 s, 10 s, and 16 s were chosen, for the refracted waves, examples at 20 s, 25 s, and 30 s. Depth values ranging from 0 km to 15 km, following the JB travel time-distance-depth tables.

The results in Table 4.3 show that for the direct waves the increasing hypocenter depth from 0 km to 15 km brings the epicenter around 3 km closer to the seismic station, independent from the delta time. Whereas, for the direct wave, the increasing hypocenter depth increases the distance from the seismic station with about 10 km at 10 km depth of the earthquake. This is also independent from the delta time.

The effects of the earthquake location in relation to increasing depth discussed in this chapter are in relation to one seismic station. With seismograms available from three and more seismic stations, like in this study the uncertainties related to depth can be minimized as show later in Chapter 4.1.7. However, for local and short distance events it is often difficult to resolve the depth (Trnkoczy et al., 2002a)

Table 4.3: Changes in epicenter distance in relation to the earthquake depth at 0 km, for different delta times and different phases, Pg, Sg as direct waves, and Pn, Sn as refracted waves (Δt is delta time in seconds).

Phase	**Earthquake depth (km)**	**Epicenter distance (km)**			**Change of epicenter distance in relation to the distance at 0 km hypocenter depth (km)**		
Pg, Sg		**Δt=1 s**	**Δt=10 s**	**Δt=16 s**	**Δt=1 s**	**Δt=10 s**	**Δt=16 s**
	0	8.53	85.32	136.52	0.00	0.00	0.00
	6	6.91	83.77	135.00	-1.63	-1.56	-1.52
	12	5.88	82.87	134.20	-2.65	-2.46	-2.32
	15	5.29	82.28	133.10	-3.24	-3.05	-2.91
Pn, Sn		**Δt=20 s**	**Δt=25 s**	**Δt=30 s**	**Δt=20 s**	**Δt= 25 s**	**Δt=30 s**
	0	161.15	212.12	263.09	0.00	0.00	0.00
	6	165.30	216.26	267.23	4.14	4.14	4.14
	12	169.44	220.41	271.38	8.29	8.29	8.29
	15	171.51	222.48	273.45	10.36	10.36	10.36

4.1.4 Horizontal seismic anisotropy

In seismology, the Earth is divided into layers, each with seismic velocities assigned. Inside a layer, the velocities assumed to be isotropic, not dependent on the direction. This assumption is valid for earthquake waves that are traveling long distances. However, for local events with short distances between the epicenter and the seismic recording stations, this assumption might be not valid anymore.

For short distances, like in this study, local differences in geology and therefore in seismic velocities might affect the analysis of the seismogram for the determination of the earthquake location. The analysis of the man-made events may show this effect (see Chapter 3.8). Further, the occurrence of fault zone in the study area might also create horizontal seismic anisotropy when waves travel parallel or perpendicular to the orientation of the faults (Bormann, et al. 2002a)

However, until now no information about seismic anisotropy is available for the study area and therefore had not taken into account.

4.1.5 Earthquake locations in relation to the seismic network

In this study, the seismic stations were set in Krabi, Phang Nga, Phuket province, with relatively short distances between the stations (the distances between Station 1 to Station 2, Station 2 to Station 4, Station 4 to Station 1 is : 22, 21, 70 and 63 km respectively). Figure 4.5 shows the locations of the earthquake events (circle points) in relation to the seismic stations. The triangle symbols represent the location of seismic stations in Phuket, Krabi and Phang Nga province (that the number 1, 2, 3, 4 is the Station 1, Station 2 Station 3 and Station 4 respectively). The polygon lines connect the seismic stations indicate the boundary of the seismic network. There are 24 earthquake events occur inside the network (14 %) and 149 events occur outside the network (86 %). The man made events occurred all inside the network boundaries.

The seismic events that occur outside the network are having the large error of the epicenter, that in generally the determination of epicenter are not expect unless the seismic gap is less than 180 degrees. The seismic gap is the largest of all angles among the lines connecting a potential epicenter with all the stations in the network that recorded the event Trnkoczy et al., 2002a.

The locations of events are determined from the geometry of the network in different directions. The locations that occur inside the network are giving most uniform location accuracy from reasonably regular grid. The worst configuration is the locations of events are occurring outside the network, it will have high error of location; the possible of event are located in a big area or on a long line. (Trnkoczy et al., 2002a; see Chapter 1.1.8).

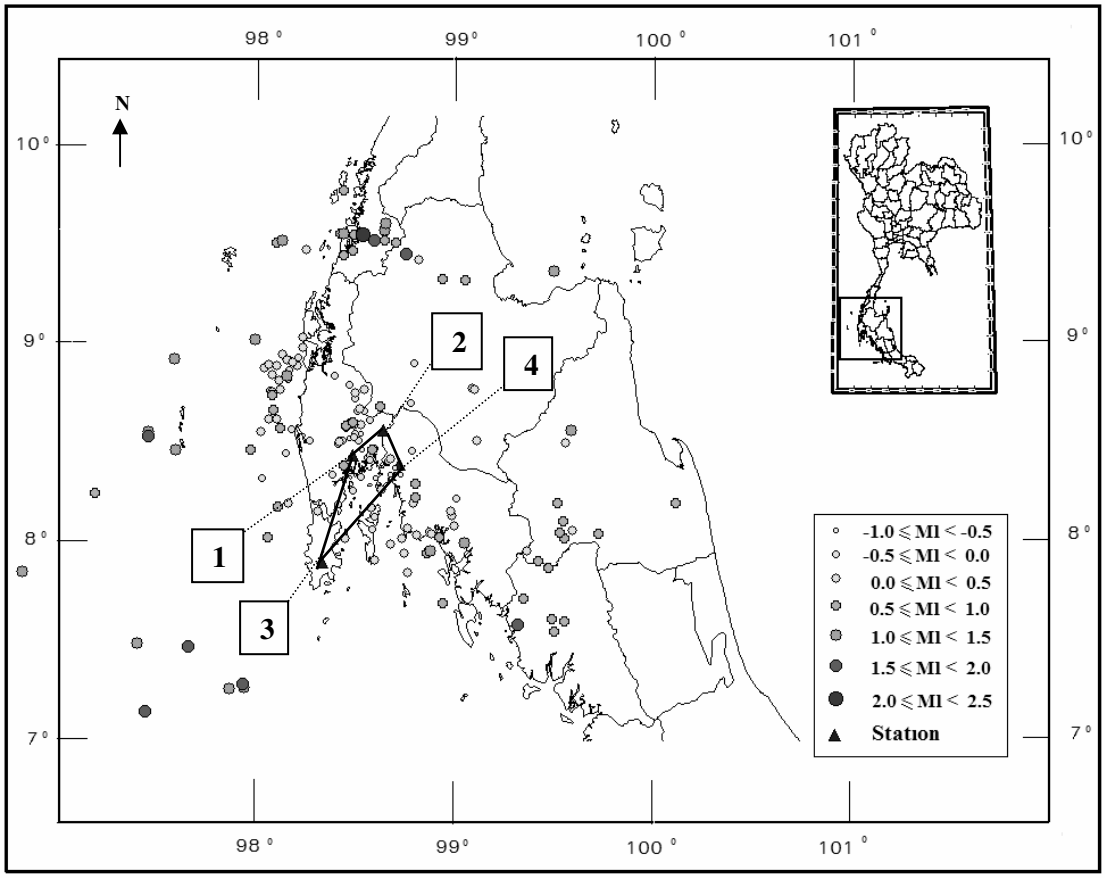

Figure 4.5. Earthquake locations in relation to the seismic network in southern Thailand. Triangle symbols show the seismic stations with the polygon as the boundary of the seismic network. The number 1, 2, 3, 4 are the Station 1, Station 2 Station 3 and Station 4, respectively.

4.1.6 Data analyzing process

A main and difficult step in the seismogram analysis of local earthquakes is the identification of the P-wave and S-wave arrival time. As the P-wave arrival is usually clear and pronounced, the S-wave arrival is often more difficult to identify. From both arrival times, the delta time between the S-wave and P-wave arrival is calculated and used for the determination of the earthquake distance. Therefore, the arrival times have a direct effect onto the earthquake location.

In the Seisan Earthquake Analysis Software the arrival times can be determined with two decimal notations of the second (hh:mm:ss.00), with Winquake Software only in one decimal notation (hh:mm:ss.0). Analyzing a seismogram with Pg and Sg phases the velocity factor for the distance determination from delta time is 8.501 km/s. A change of the delta time in 0.01 s would change the distance in 85.0 m, a change in 0.1 s would change the distance in 850 m. A similar relation can be found for the refracted waves, but with larger distances (Chapter 2.11.1).

The analysis of the man made events provides an insight in the quality of the arrival time determination. The seismograms from Station 1 and Station 2 were analyzed for these events. The exact location of the sources is not proven. For a discussion see Chapter 4.4. The source is believed to be blasting in a limestone quarry, about 10 km to 12 km from both stations (see Nilsuwan, 2006; Chapter 4.4). It can be assumed that the source is not a point source, rather several sources distributed over a small confined area, probably not more than 500 to 1,000 m in length and width.

The analysis of the arrival times of the P- and S-wave as done with Seisan Software for all three components, using 37 seismograms from each seismic stations for the same events (see Figure 4.6, Nilsuwan, 2006). The results show that the calculated average values of the delta time for different components from each station have small differences; maximal 0.034 s for Station 1 and maximal 0.003 s for Station 2 (see Table 4.4). Further, the standard deviation of the delta time from using all three components is 0.052 s for Station 1 and 0.044 s for Station 2.

Additionally, these data show that the standard deviations from the average value for all components or only for the Z-component, which is usually only used in the analysis, are between 0.042 s and 0.052 s. Converted into distance by using the JB tables for 0 km hypocenter depth this would be 0.357 km to 0.442 km.

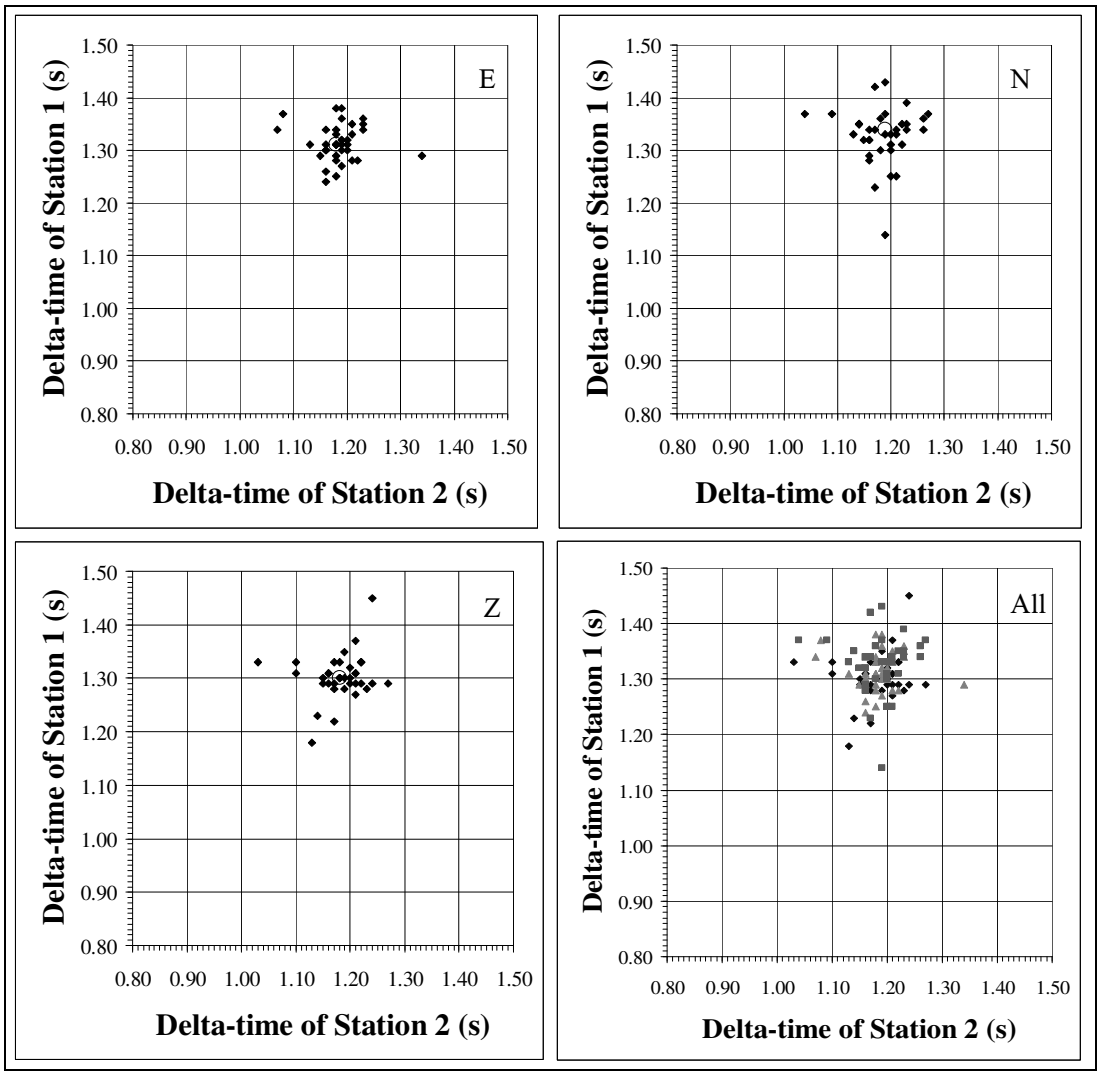

Figure 4.6. Relationship between the delta-times (in seconds) from Station 1 and Station 2 for all 37 man made events for the E-, N-, Z-component, and all three components together. The circles indicate the average delta-time of the each component, respectively of all components (after Nilsuwan, 2006).

Table 4.4: The average and standard deviation (STDEV) for delta times (Δt) of the E-, N-, and vertical Z-component for all 37 man made events recorded at Station 1 and Station 2 (after Nilsuwan, 2006).

components	Δt (s)			
	Station 1		Station 2	
	Average	STDEV	Average	STDEV
E	1.314	0.034	1.184	0.043
N	1.336	0.071	1.185	0.047
Z	1.302	0.042	1.182	0.045
All	1.318	0.052	1.184	0.044

4.1.7 Number of recording stations

In this study, most of the earthquake locations were determined using data from three seismic stations, which is sufficient, see Chapter 1.1.8 (Bormann and Wylegalla, 2002a). However, due to missing data earthquake locations were also determined using data only from two or even one seismic station. Details of the procedures are given in Chapter 2.11. With a decreasing number of seismic stations, the uncertainty of the location increases (Bormann and Wylegalla, 2002a).

With two station data, there will be two possible locations as shown in Figure 4.7. This could be resolved with additional back azimuth determinations, if the two solutions are not relatively close. With one station the location rely solely on the distance information from delta time measurements and back azimuth determination. This can provide relatively good location data, as shown by Choowong, 2007 for the 26 December 2004 Mw 9.3 and 28 March 2005 Mw 8.7 Earthquake. With three-component single seismic station data, the locations were in good agreement with USGS and EMSC location information. Nevertheless, the back azimuth method is sensitive to any non-distance related amplitude change, for example by geology changes or anisotropy of seismic wave velocities, and therefore would give errorness locations.

Using data from three seismic stations, the determined location still might give not an exact solution. The main uncertainty comes from the identification of the phases and the determination of the arrival times, for the local earthquakes of this study, mainly the S-wave arrival (Trnkoczy et al., 2002a).

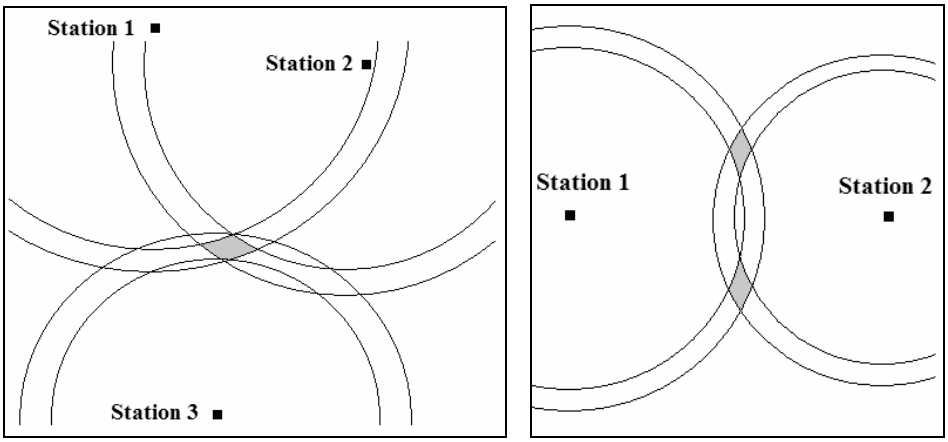

Figure 4.7. Schematic figure of the location determination of earthquakes and its uncertainty with three (left) and two (right) seismic stations. The distance determined from the delta time of each station has an uncertainty, which is indicated by the area between two parallel circles with a different radius from each station. For three stations all six circles will bound an area, which gives the location of the earthquake. The size of the area indicates the uncertainty of the location. With two seismic stations, two areas, each bounded by four circles, show the possible locations of the earthquake. Additional information is needed for the determination of the final location, like the back azimuth from one or two stations.

4.1.8 Earthquake location in respect to fault orientation

The identification of faults is essentially based on geological field studies, where a displacement on two sides of the fault plane could be identified. The relative orientation of the fault plane in relation to the rock units is defined by its tectonic style (e.g. strike slip fault, normal fault, and reverse fault, see Chapter 1.4. Besides the extent of the fault, geological mapping can reveal the orientation of the fault, with its strike and sip angle. However, this is limited in to areas with rocks exposed at the surface. In areas where this access is limited, morphological studies of the Earth's surface also can reveal faults, for example differences in the elevation, or changes in the river system (Haller, 2007). For these studies often airborne or satellite

images are used. However, these methods can only determine the strike of a fault, usually not the fault dip.

The faults identified in Southern Thailand are mainly based on morphological differences at the surface, some on geological studies, including the Khlong Marui and the Ranong Fault Zones (Garson and Mitchell, 1975, Keller, 2000, Charusiri and Pailople, 2007). The dip angle of these faults if often not know, because the fault planes are not exposed at the surface due to the weathering of the near surface rock units.

Earthquakes along active faults not necessarily rupture along perfect planes, rather in rectangular or circular areas. Real faults, like the Khlong Marui and Ranong Fault Zone, usually have jogs, steps, branches, and splays in their horizontal and vertical extent (see Figure 4.8, also Figure 1.17 in Chapter 1.1.6). Earthquakes generate from complex faults can show multiple ruptures. This holds true for small magnitude earthquakes as well as very large ones (Kikuchi and Fukao, 1987, Kikuchi and Ishida, 1993).

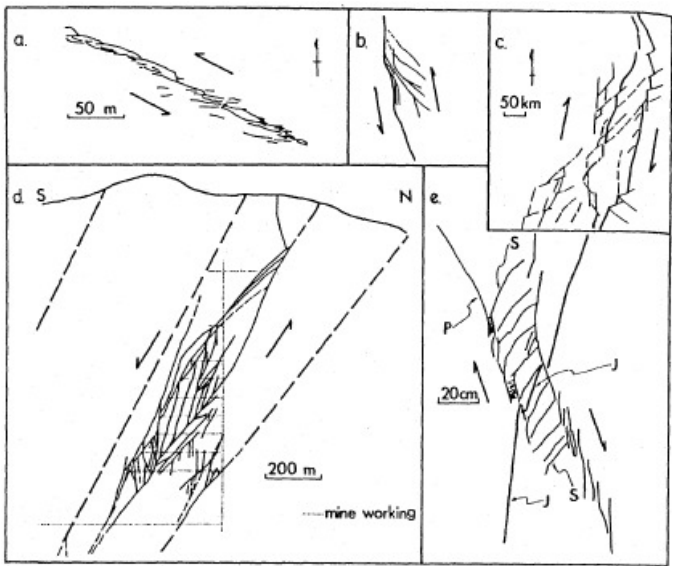

Figure 4.8. Several fault zones mapped at different scales and viewed approximately normal to slip (from Scholz, 1990).

The rupture at a fault defines the earthquake location. When a rupture at a fault occurs at a certain depth (hypocenter), the epicenter location will be away from the surface expression of the fault as shown in Figure 4.9. Figure 4.10 provides quantitative values for an earthquake at 10 km depth and for a fault with different dip angles. At a dip angle of 15 degrees, the epicenter is 37.32 km away from the surface expression of the fault. With increasing dip angle, the distance decreases, with 5.77 km at 60 degree dip angle.

In a fault zone with closer spaced parallel faults, as shown in Figure 4.11, the epicenter of an earthquake generated at a depth at fault B1 can be located on the surface expression of the fault B2. This may lead to wrong interpretations of the fault type, seismic active or not. Further, an earthquake can be generated at fault, which shows no surface expression, so called "hidden fault". Any correlation of such an earthquake with a fault will fail. All these possibilities regarding the relationship between faults and earthquakes, including the existence of hidden faults, have to be expected in the study area.

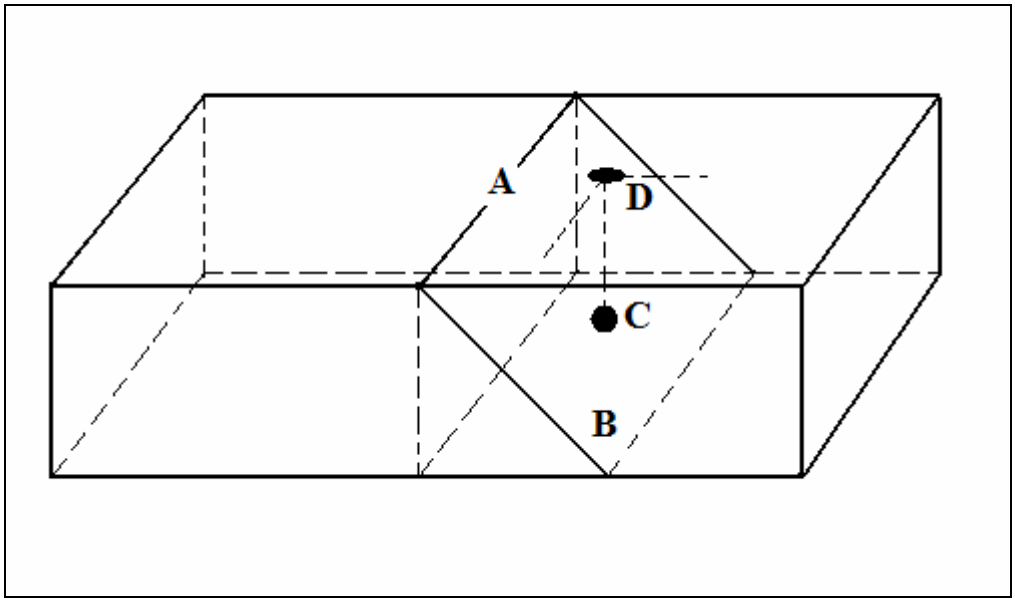

Figure 4.9. Schematic diagram of relationship between fault plane (B) and its surface expression (A), the hypocenter of an earthquake (C) and its epicenter (D). The epicenter is away from the surface expression of the fault.

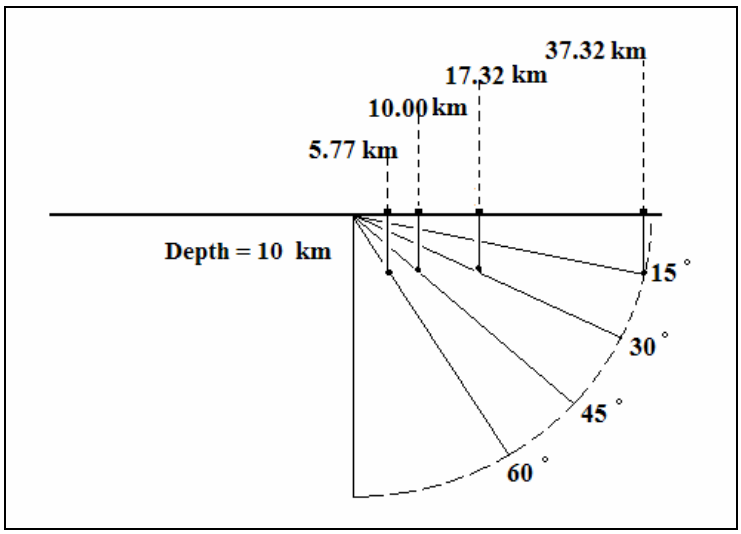

Figure 4.10. Schematic layouts of the distance between epicenter and surface expression of a fault for different dip angles of the fault, 15 to 60 degrees. The hypocenter is always at 10 km. The distances between the surface expression of the fault and the epicenter decreases with increasing dip angle of the fault.

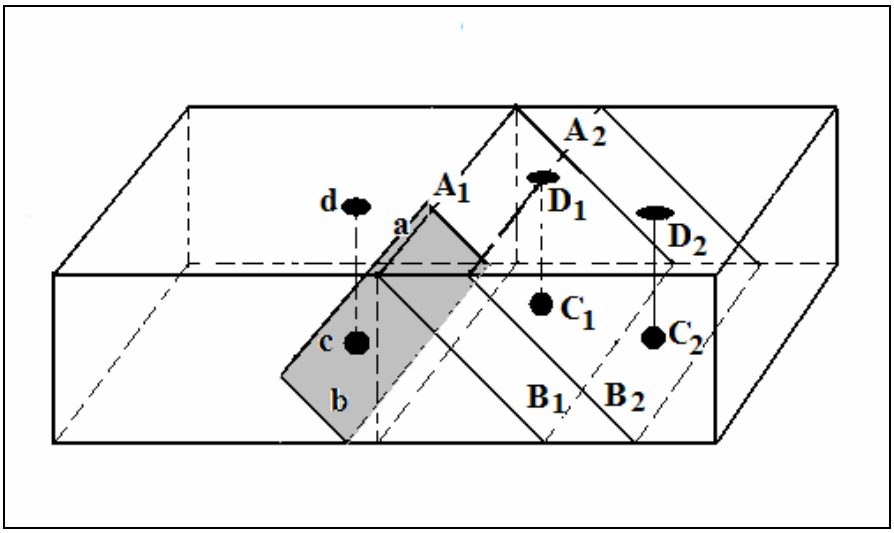

Figure 4.11. Schematic diagram of relationship between fault planes in a fault zone (B1 and B2) and their surface expression (A1 and A2), the hypocenters of the earthquakes (C1 and C2) and their epicenters (D). The epicenter C1 lies on the surface expression of the fault A2. The hidden fault (b) has no surface expression, so that the earthquakes epicenter d (hypocenter c) cannot be correlated to any fault.

4.1.9 Local Magnitude

Since there is no amplitude-distance correction factor of Southern Thailand available. The magnitude formula of southern California area (Hutton and Boore, 1987) was therefore used to determine magnitude of local earthquakes in this study area.

The use of the Hutton and Boore (1987) formula means, that the determined magnitudes values might be different in case an amplitude-distance correction factor for Southern Thailand would have been used. However, this uncertainty will stay until detailed investigations in the attenuation correction factor for Southern Thailand have been carried out.

Further, 59 events of all the earthquakes measured in this study have negative magnitude values. This is well known, as the local magnitude scale was introduced using data from the analog Wood-Anderson seismograph. Earthquakes with negative magnitude are called "nano earthquakes". Most of these earthquakes have relative small distances from the recording stations, in some cases below 10 km.

Following Joswig (2007) the standard local magnitude determinations fail for nanoseismic events, because the monitoring is not intended to handle events of small amplitudes and of short slant distance. To preserve the relation to the microseismic event scale (Ml more than 0), he introduces an extended concept of Ml calculation suited for ultra-small events. The magnitudes are corrected from distance and maximum amplitude plots, where the slope of the distance correction must match all data to define a common magnitude.

In the original Richter (1958) magnitude for local earthquakes, the amplitude-distance correction factor for events with distances smaller than 10 km is nearly flat: $\sigma L(\Delta)$ for 10 km is 1.5, for 0 km is 1.4 (Bormann, 2002b). After Joswig (2007) "[this] slope of zero for the original definition of Richter (1958) is simply unreasonable". From his own calibration measurements at short distances to the source, with 30 m, 100 m, and 300 m, he provides a slope of -log(A0) = -1 for the amplitude-distance correction below 10 km source-receiver distance.

In this study, no calibration measurements for these short distances have been carried out. However, the use of the Hutton and Boore (1987) formula for local earthquakes provides amplitude-distance correction factors for infinite (short) distances. For source-receiver distances between 10 km and 1 km the values give a slope of -log(A0) = -1.127, see Figure 4.12. This value might be not necessarily true for the study area, but it is a reasonable value in comparison to Richter (1958) and Joswig (2007).

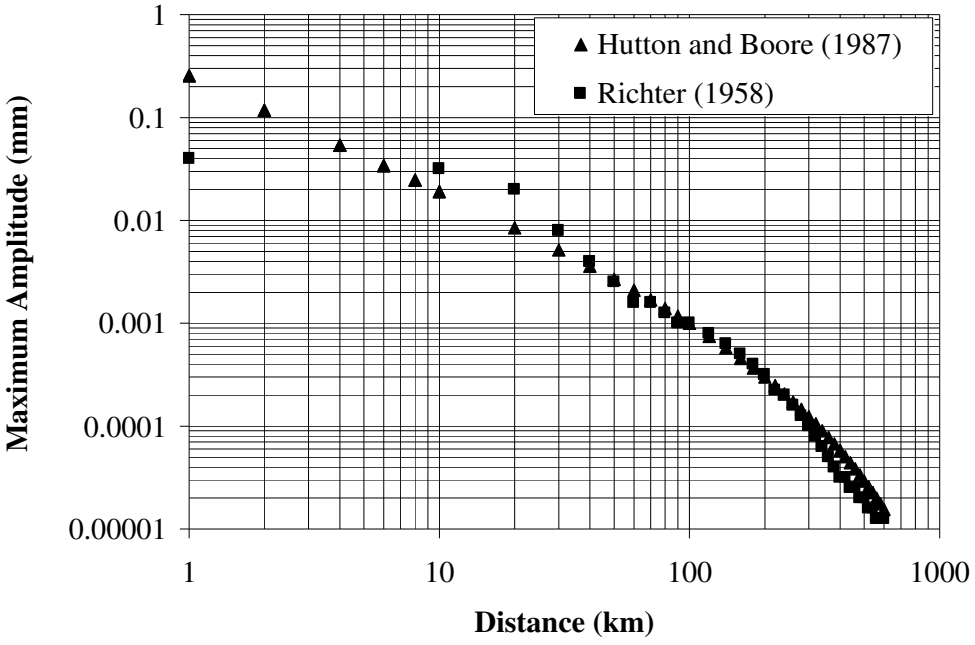

Figure 4.12. The amplitude-distance correction of the original Richter formula (Richter, 1958) and the Hutton and Boore formula (Hutton and Boore, 1987). That the amplitude-distance correction factor for events with distances smaller than 10 km is nearly flat for the original Richter formula, but the slope of -log(A0) is -1.127 for the Hutton and Boore formula.

4.1.10 Summary of uncertainties

The main earthquake parameters are origin time, location and magnitude for the local earthquakes in this study. They depend primarily on the identification and analysis of the P- and S-phase, as outlined in Chapter 2 and 3. However, other factors also have an effect on the earthquake parameters as shown in the previous chapters. Therefore, as shown and discussed above, all the main earthquake parameters come with an uncertainty. In addition, attempts were made to quantity the uncertainty related to individual factors. However, final quantitative values for the main earthquake parameters cannot be given, as individual factors can have contrary effects. Further, a correlation of earthquake locations with faults or fault zones, as done in the coming chapter, also has to acknowledge uncertainties in the existence of a fault, e.g. hidden fault, and the fault location itself.

4.2 Correlation of earthquake locations within faults

The results of this study have shown that after the 26 December 2004 Mw 9.3. Andaman-Sumatra Earthquake earthquakes occurred in Southern Thailand. A main objective of this study was the question, whether these earthquakes are related to existing and known faults and faults zones, especially the Ranong and the Khlong Marui Fault Zone.

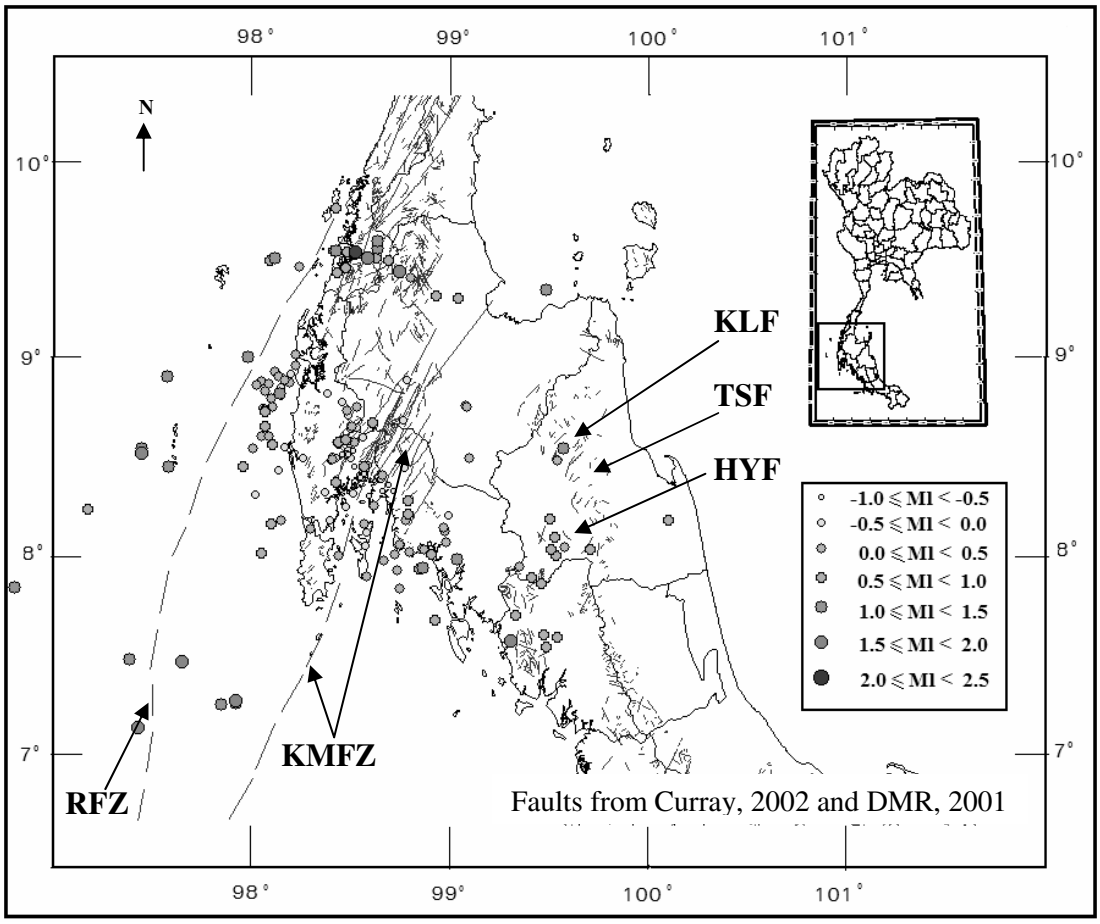

Figure 4.13. Map of Southern Thailand with the 173 earthquake locations determined in this study and the known locations of faults and faults zones (from Curray, 2002 and DMR, 2001) RFZ: Ranong Fault Zone, KMFZ: Khlong Marui Fault Zone, KLF: Khao Luang Fault, TSF: Thung Song Fault and HYF: Huai Yot Fault. The earthquake locations have different symbols in relation to their local magnitude, presented in classes of 0.5 values.

All the locations of the 173 earthquakes determined in this study in relation to the surface expressions of known faults and fault zones are shown in Figure 4.13. From the distribution, it can be seen that some of the earthquakes might follow existing faults, especially in the Northwestern part parallel to the Ranong Fault Zone.

Figure 4.13 gives a more detailed view of the area. Several earthquakes are following a SW-NE trend parallel to the Ranong Fault, which might be part of the Ranong Fault Zone (Fault F1 in Figure 4.14). However, several earthquakes might be located on a fault with a NW-SE trend, Fault F2. Garson and Mitchell (1975) have shown that this trend in general is possible for faults in this area, e.g. the Klong Sok Fault further South in Phang Nga area shows also more East-West trend.

In the Andaman Sea offshore Ranong and Phang Nga Province, several earthquakes also follow a fault like linear trend, F3 fault in Figure 4.15. This might be also a fault related to the Ranong Fault Zone. However, for these correlations it has to taken into account that the line of the map named Ranong Fault Zone might not be the true location or the fault zone is much wider than anticipated.

Further south, several earthquakes also might follow linear trends, which might be faults, like F4 fault in Trang and Nakhon Si Tammarat Province it further south of the Khlong Marui Fault Zone and align on SW-NE trend, which is parallel to the Ranong and Khlong Marui Fault Zone. F4 fault might be correlated with known faults in its vicinity, like the Khao Luang Fault, Thung Song Fault, and Huai Yot Fault.

A characteristic of all the faults discussed here, F1 to F4 fault, is that they are several hundreds of kilometer long. In this way, they only can be compared with the prominent Ranong and Khlong Marui Fault Zone. All other known faults are much shorter (see Figure 4.13 and 4.15). However, there are also much further north and south than both of the major fault zones.

Further, several earthquake locations do not show and obvious linear trend than the ones discussed above. They are mainly located in the Phuket, Phang Nga and Krabi area, outlined as cluster C1 area.

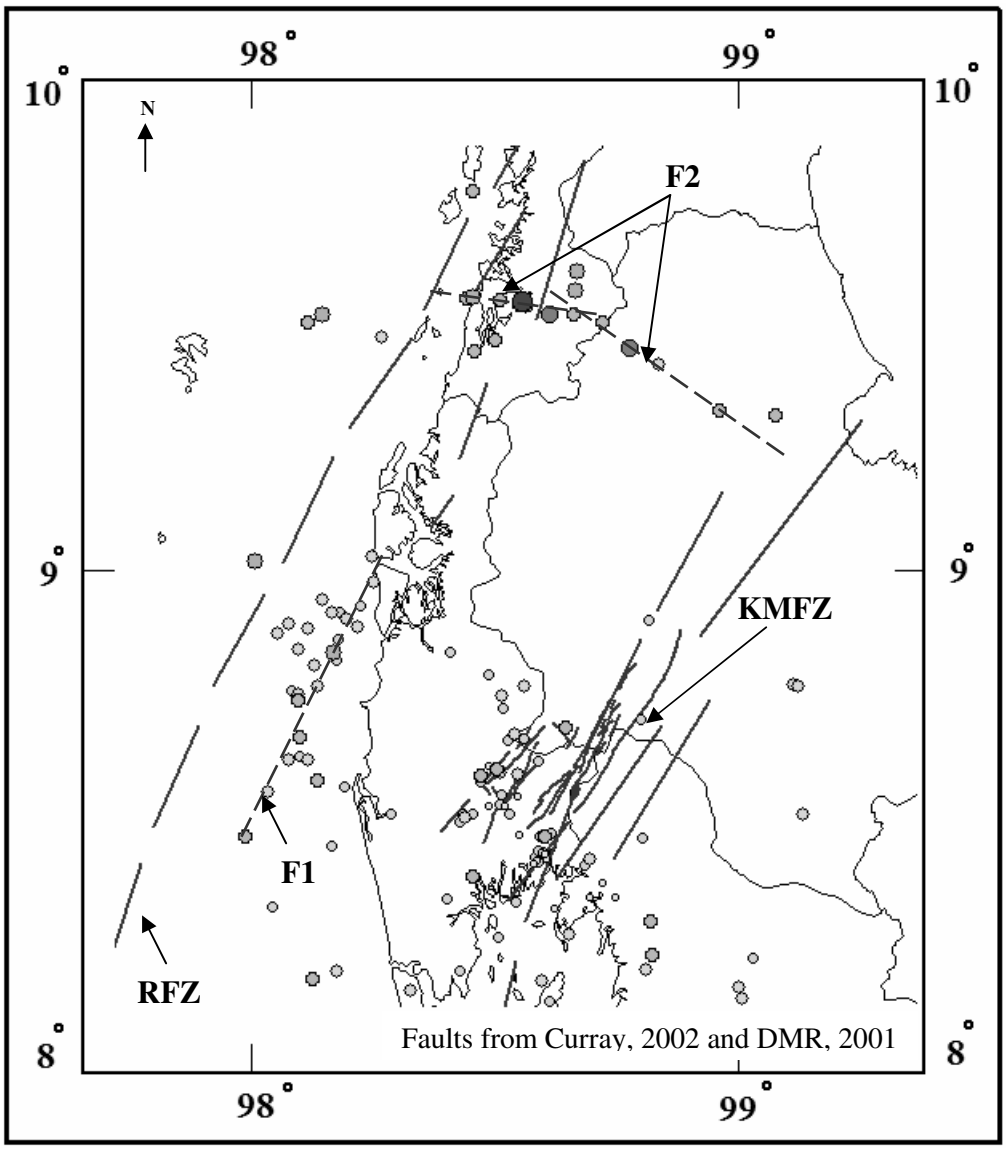

Figure 4.14. Detailed view of the northwestern part of Figure 4.13. The earthquake locations have different symbols in relation to their local magnitude, presented in classes of 0.5 values (see Figure 4.13). F1 is the trend of earthquake location that align on SW-NE parallel to the Ranong Fault and F2 are the trend of earthquake location that align on NW-SE. RFZ and KMFZ is the Ranong Fault Zone and Khlong Marui Fault Zone respectively, (Fault zone are located from Curray, 2002 and DMR, 2001).

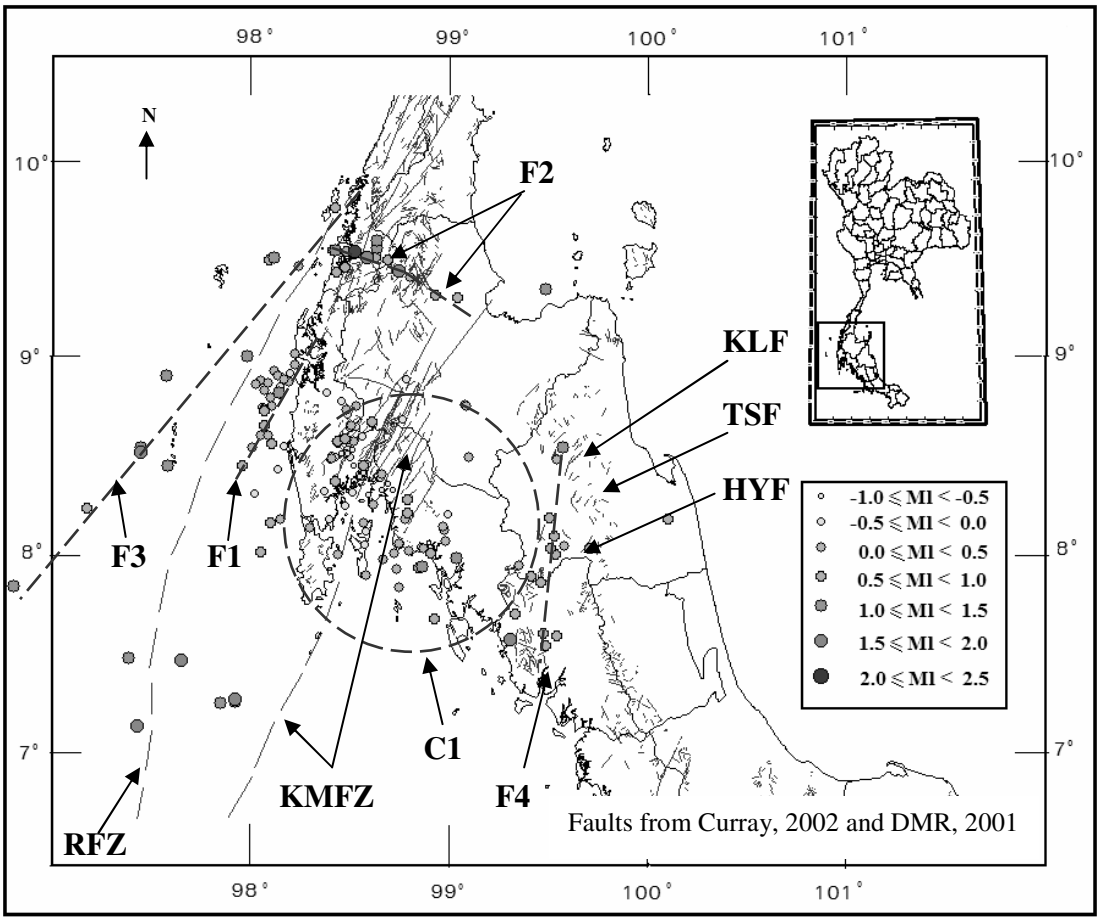

Figure 4.15. Map of Southern Thailand with the 173 earthquake locations determined in this study and the known locations of faults and faults zones (Curray, 2002 and DMR, 2001). The earthquake locations have different symbols in relation to their local magnitude, presented in classes of 0.5 values. RFZ, KMFZ, KLF, TSF and HYFis the Ranong Fault Zone, Khlong Marui Fault Zone, Khao Luang Fault, Thung Song Fault and Huai Yot Fault. F1, F2, F3, and F4 are trends of earthquake location that can be on faults and C1 is the cluster of earthquake locations.

4.3 The origin of earthquake in southern Thailand after the 26 December 2004

As discussed in the previous chapter, several local earthquakes measured during this study in Southern Thailand after the 26 December 2004 Earthquake might be related to faults, respectively their movement, some might be not. However, the crustal movement related of the Mw 9.3 earthquake can be used to explain the occurrence of all earthquakes.

Before the 26 December 2004 Earthquake, the Indian-Australian Plate and the Eurasian Plate were locked at the subduction zone in the Andaman Sea area with the Indian-Australian Plate moving 50 to 60 mm to NNE (see Chapter 1). Therefore, the Indian-Australian Plate pushed the Eurasian Plate with the small Burma Plate also to the NE. Data from a Global Positioning System network in SE Asia has shown this movement (Hashimoto et al., 2006a, see Figure 4.16 and 4.17).

Because of this, the Eurasian Plate deformed near the subduction zone trench with shortening and uplift (see Figure 4.16A). Also further to the East, the lithosphere of the Eurasian Plate was compressed due to the pushing of the Indian-Australian Plate. This might have lead to movements along the Ranong and Khlong Marui Fault Zone. The earthquake on Ranong Fault 30 September 1978 with magnitudes 5.6 (Nutalaya, 1994) might be the result of this.

With the 26 December 2004 Mw 9.3 Earthquake, the Indian-Australian Plate and the Eurasian Plate with the Burma Plate unlocked (see Figure 4.16B). This resulted in an immediate coseismic movement of the Eurasian Plate to the West with a smaller South-component. The GPS data from the Station on Phuket, Thailand, show that the station moved 26 cm to the WSW during the Mw 9.3 Earthquake (See Figure 4.17 and 4.18). This was the largest movement measured after this earthquake in comparison to stations in Thailand, Malaysia and Indonesia (see Figure 4.18).

The Sampari Station in Northern Sumatra and a station in Chumpon, between Phuket and Bangkok, moved during this earthquake about 12 to 13 cm to the West with a small South-component (See Figure 4.17 and 4.18). GPS stations in Malaysia also moved much less to the West compared to the Phuket Station in Thailand (Vigny et al., 2005).

The higher movement values for Phuket after the 26 December 2004 Earthquake can be explained with a differential movement of this area along the Khlong Marui Fault Zone in the South and Ranong Fault Zone further north. GPS stations north and south of these fault zones show smaller movement values.

This differential movement along the fault zones resulted in earthquakes along these faults as shown in Chapter 14. However, earthquake data for Southern Thailand are available from 14 January 2005, so that an increase of the earthquake activities in this area after the 26 December 2004 can be only assumed (See Figure 4.19).

Nevertheless, since the 14 January 2004 there was a sharp increase in the number of earthquakes, until the 21 January 2005 (see Figure 4.19). After that, only four earthquakes were recorded until 1 March 2005. The change in the earthquake numbers can be correlated with the GPS data. After the 26 December 2004, the movement to the SSW went further, about 6 cm until 21 January 2005. With this date the movement nearly stopped in both directions, east and south, giving a nearly flat line in the GPS data (see Figure 4.19). Mid of February the movement started again at a much slower rate, especially in the East-component.

The earthquake activities started again on 1 March 2005 with a sharp increase in the cumulative number. With increasing time, the slope of the increase slowly decreases in a logarithmic trend.

The 28 March 2005 Mw 8.7 Earthquake, with a location further south of the 26 December 2004 epicenter, had only a little effect on the GPS movement at the Phuket Station. The station moved more south than west, but altogether only 1 to 2 cm. In contrast, the Sampari Station on Sumatra Island moved on 28 March 2005 about 14 cm to the West and the South, altogether nearly 20 cm (Figure 4.17 and 4.18).

The small movement values for the Phuket Station might explain that the 28 March 2005 event did not result in an increase of the number of local earthquakes in Southern Thailand, what might have been expected in comparison to the 26 December 2004 event.

Before, during and after the 26 December 2004 the Gravity Recovery and Climate Experiment (GRACE) twin satellites measured the gravitational

acceleration in the Andaman Sea area (Han et al., 2006). They observed ±15-microgalileo gravity changes induced by the 26 December 2004 Earthquake. These gravity changes were explained with coseimic deformation: a) the vertical displacement with subsidence and uplift of the lithosphere of the Eurasian Plate near the subduction zone trench (see Figure 4.16B), and b) the dilation of the compressible lithosphere of the Eurasian Plate with changes in crustal and upper mantle densities. This internal mass distribution is the result of the stress relief inside the Eurasian Plate after the 26 December 2005 Earthquake unlocked this plate from the subducting and pushing Indian-Australian Plate (see Figure 4.16B).

This dilation process after the 26 December 2004 Earthquake can explain also in parts the occurrence of local earthquakes in Southern Thailand. The stress relief after the expansion of the compressed crust of the Eurasian Plate is associated with small-scale movements. These movements result in low magnitude earthquakes, which are not associated to fault zones, as observed in this study (see Figure 4.15, C1 cluster). As the stress regime after the 26 December 2004 Earthquake is extensional in comparison to compressional before, no medium to high magnitude earthquakes could be expected (see Figure 4.16B).

After the 26 December 2004 Earthquake, an initial relaxation phase with horizontal movement to the West resulted in local earthquakes in Southern Thailand before 21 January 2005. The increase of earthquake occurrences after 1 March 2005 associated with a sharp increase in the number of earthquakes might represent a second relaxation phase. However, this second relaxation phase is not associated with substantial movement of the plate to the west, as shown by the GPS data, but relaxation of the plate itself.

The dilation process in the Eurasian Plate also resulted in the increase in sinkhole occurrence in Southern Thailand (see Figure 4.19). Sinkholes are natural phenomena in areas with limestone or evaporate rock formations in the subsurface, like in many parts of Southern Thailand. An increased number of sinkhole occurrences were reported after the 26 December 2004 Earthquake. The dilation processes associated with the Mw 9.3 Earthquake resulted in mechanical unstable roofs of subsurface holes and the subsequent subsidence. Further interpretation of the sinkhole data is limited, as not all sinkholes might have been reported and the time of

the report used in Figure 4.19 is not necessarily similar with the time of the occurrence.

As an outlook for the future, GPS data will show one day that the interface between the Indian-Australian Plate and the Eurasian Plate, which was unlocked by the 26 December 2004 Earthquake, will be locked again. Then the Indian-Australian Plate will push the Eurasian Plate again to the East. The lithosphere of the Eurasian Plate will be compressed and deformed again (see Figure 4.16A). In this compressional stress regime higher magnitude earthquakes in Southern Thailand are possible through the reactivation of the Khlong Marui, Ranong and other fault zones.

Figure 4.16. (next page) The model of the 26 December 2004 Earthquake. That the small picture at the left are the cross section of the subduction zone (from Hyndman and Wang, 1993) and picture at the right is the zooming of area. The reticules show the compress (stress) in that area and the arrows are the directions of plate moving. ‘A’ is the model of plates before the 26 December 2004 Earthquake, ‘B’ is the model of plates after the 26 December 2004 earthquake.

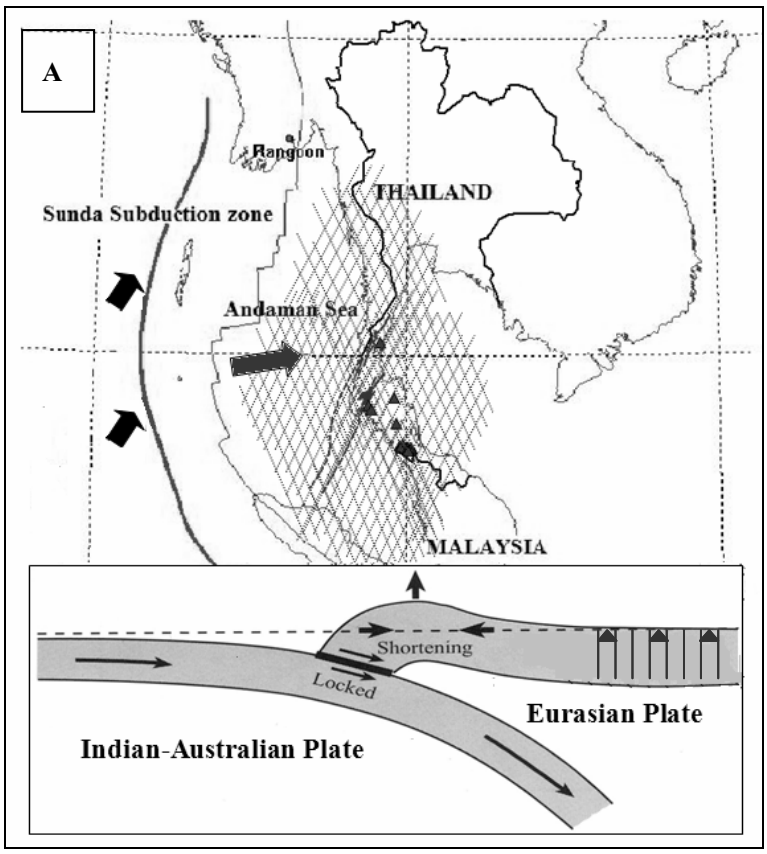
A
Rangoon
THAILAND
Sunda Subduction zone
Andaman Sea
MALAYSIA
Shortening
Locked
Eurasian Plate
Indian-Australian Plate

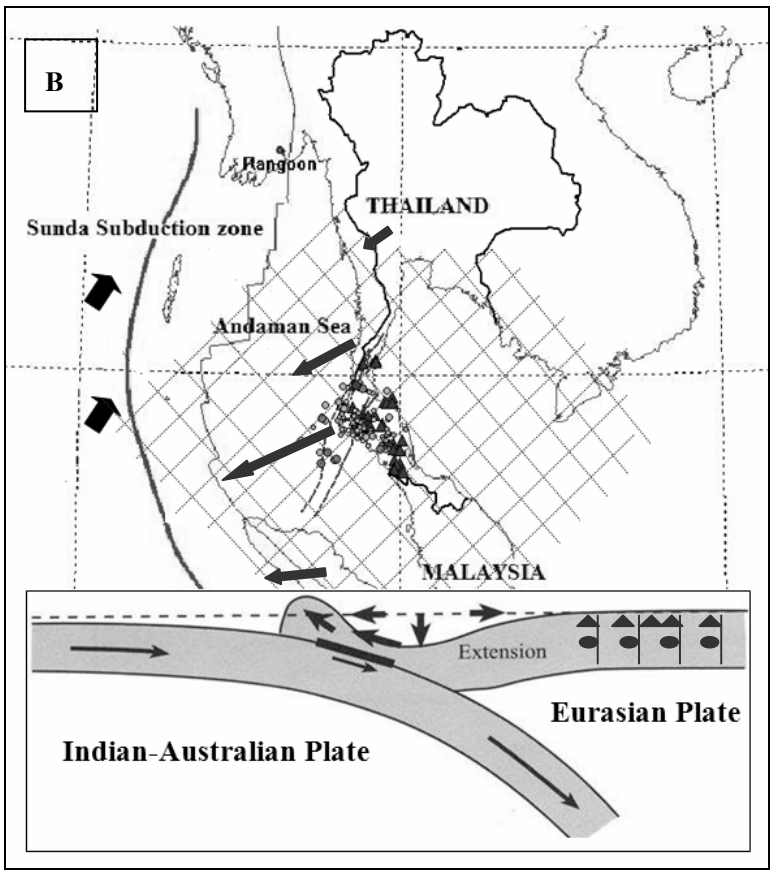
B
Rangoon
THAILAND
Sunda Subduction zone
Andaman Sea
MALAYSIA
Extension
Eurasian Plate
Indian-Australian Plate

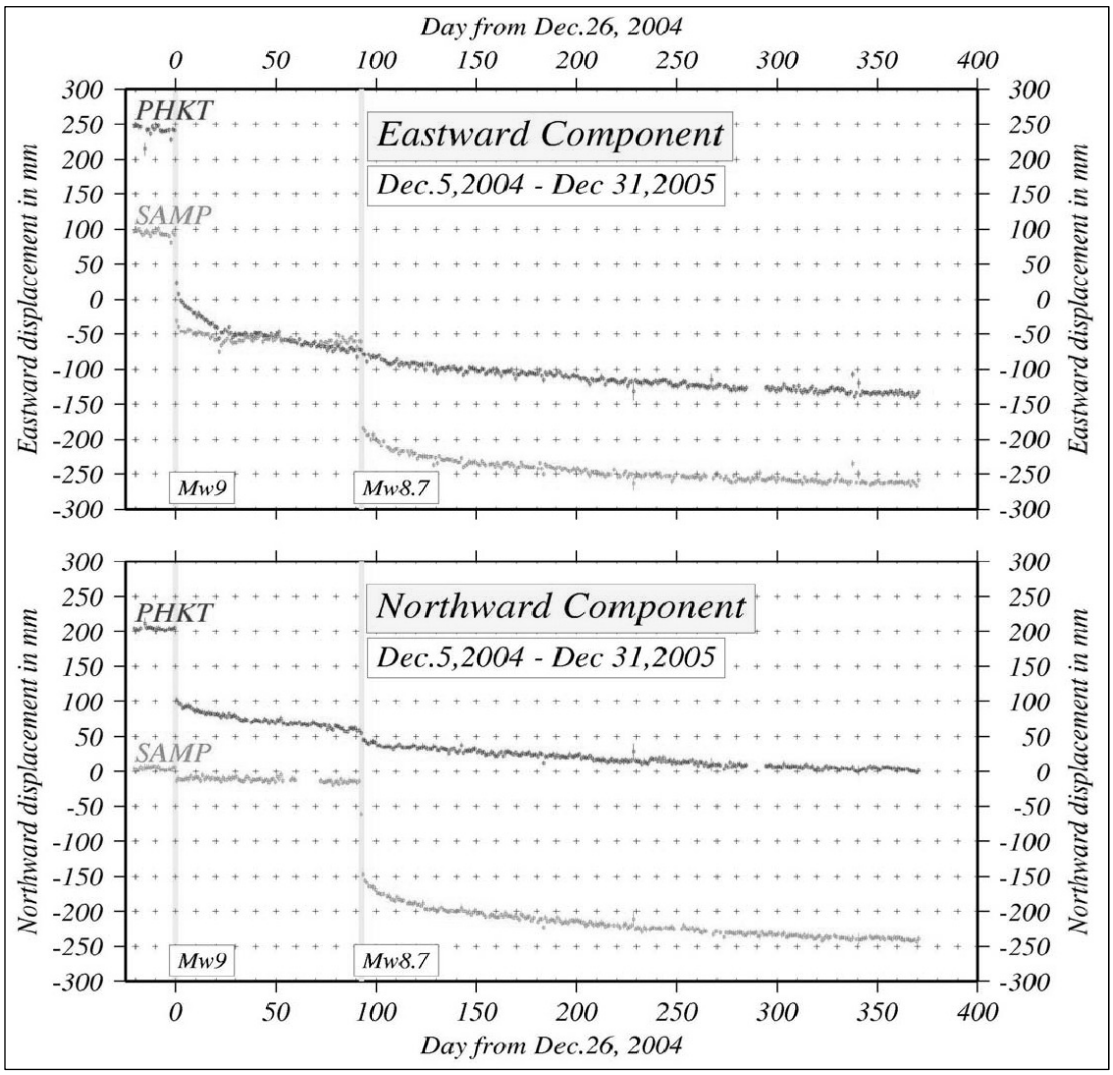

Figure 4.17. The time series, in days after the 26 December 2004 Earthquake, of coordinate changes, in mm at the Phuket (PHKT) and Sampari (SAMP) GPS stations from 5 December 2004 to 31 December 2005. Top: Eastward component and bottom Northward component (from Hashimto et al., 2006b).

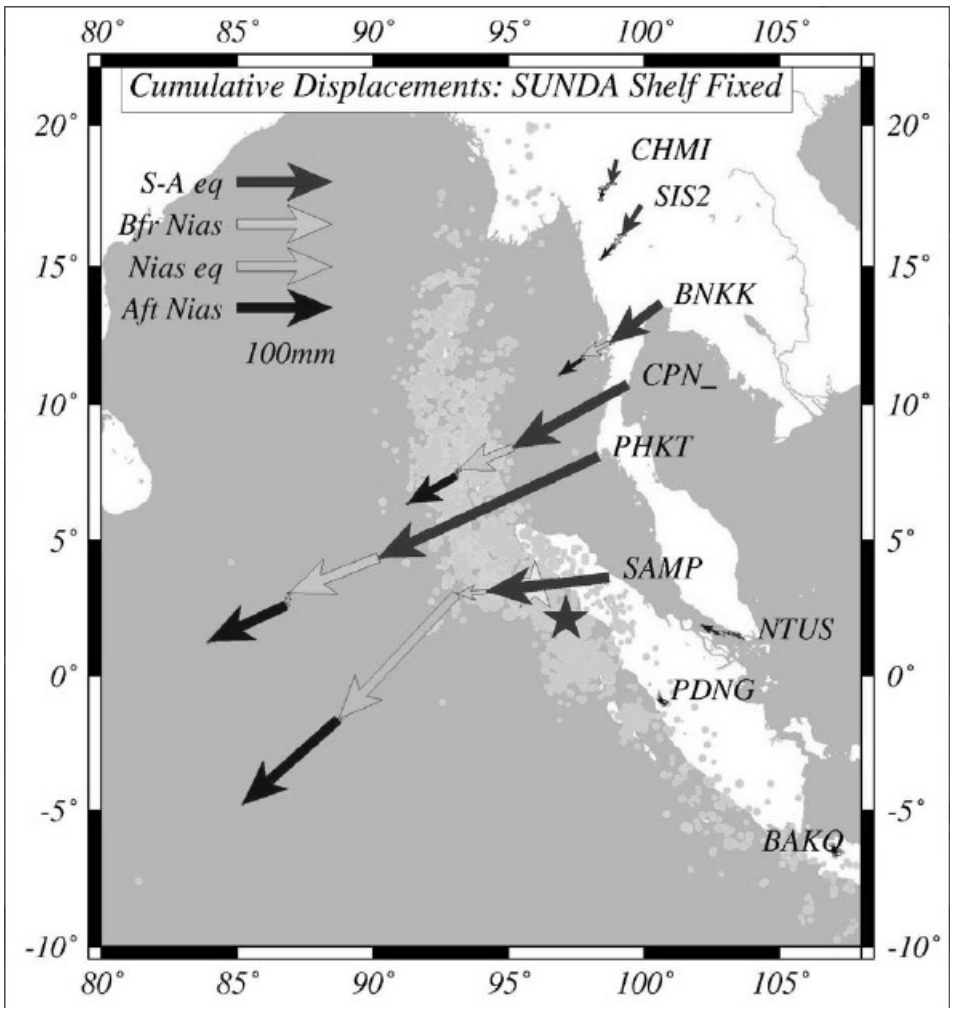

Figure 4.18. Cumulative displacement of the lithosphere during the 26 December 2004 Earthquake (S-A eq), before the 28 March 2005 Earthquake (Bfr. Nias), during the 28 March 2005 Earthquake (Nias eq), and after the 28 March 2005 Earthquake (Aft Nias) until 31 December 2005. Stars show the locations of the 26 December 2004 Earthquake and the 28 March 2005 Earthquake. Arrows indicate the value and direction of displacement (from Hashimoto et al., 2006b).

Figure 4.19 (next page) The relation of the displacement of Phuket GPS Station (see Figure 4.18, after Hashimoto et al., 2006a), the cumulative number of local earthquakes (this study) and sinkholes in southern Thailand (DMR, 2005) with time. The origin time of the 26 December 2004 and 28 March 2005 Earthquake are indicated, as well as important dates (see text).

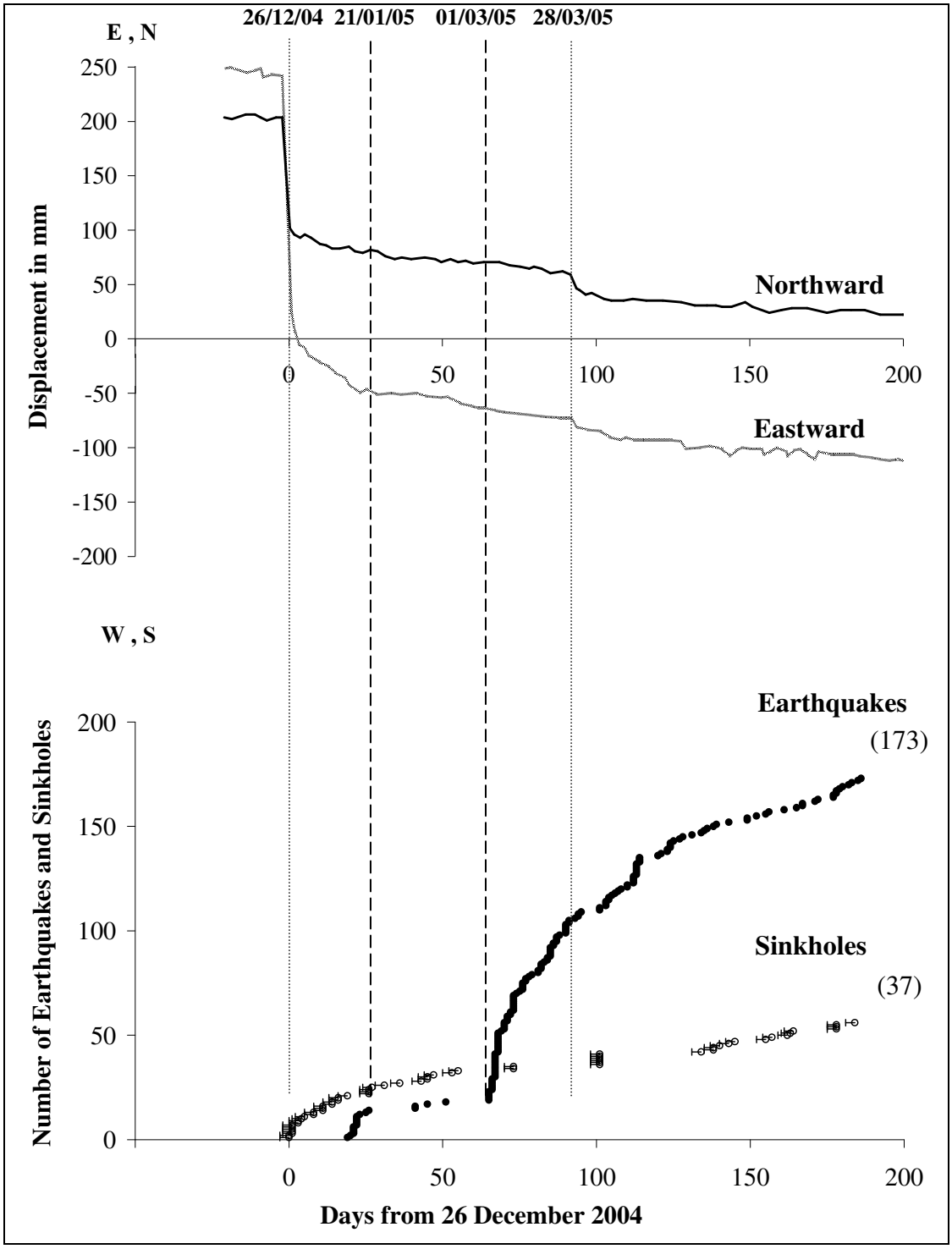
26/12/04
21/01/05
01/03/05
28/03/05
E , N
Displacement in mm
250
200
150
100
50
0
-50
-100
-150
-200
Northward
Eastward
0
50
100
150
200
W , S
Number of Earthquakes and Sinkholes
Earthquakes
(173)
Sinkholes
(37)
Days from 26 December 2004

4.4 The origin of the man-made events

In this study, 37 man made events have been identified in the area of Phang Nga. Nilsuwan (2006) determined the average location of these events at UTM Zone 47, 939497 N and 454576 E (WGS-84). Although, no source of these events has be found in this area, it is very likely that the source might be a rock quarry with blasting activities, which can be found often in this area (See Nilsuwan, 2006). The low magnitudes of these events (almost all below Ml 0.0) might be a further indication for that.

Nevertheless, there are four limestone quarries in the area, which might be the possible source of the events with following locations (see Figure 4.20; Nilsuwan, 2006; all locations in UTM, Zone 47, WGS-84): Quarry A (453350 E, 936635 N), Quarry B (451450 E, 936625 N), Quarry C (453350 E, 936440 N), and Quarry D (455865 E, 944695 N).

In a detailed study, Nilsuwan (2006) concluded that for these short distances between the seismic stations and the seismic source, 10 km to 12 km, differences in the subsurface rock formations might have an effect on the determination of the source location.

In the subsurface of the area between the seismic Station 1 and the average location of the man-made events there is mainly limestone as indicated by the distribution of limestone outcrops (see Figure 4.20). Whereas sandstone in mainly in the subsurface of the area between the seismic Station 2 and the average location following the outcrop distribution.

Therefore, the seismic waves travel to Station 1 mainly through limestone, whereas to Station 2 mainly through sandstone. However, the Vp/Vs ratio for limestone is 1.89 and 1.50 for sandstones, following Schoen (1996). In this situation, the use of the average crustal velocities of the JB or any other velocity model might not be appropriate any more.

Modifying the velocities with Vp=5.90 km/s and Vs=3.13 for the seismic waves traveling to Station 1, and with Vp=5.75 km/s and Vs=3.42 km/s for the waves traveling to Station 2, Nilsuwan (2006) concluded Quarry C as the location

of the man-made events. Using blasting techniques, the limestone is mined, then crushed and used for construction purposes.

The construction material was needed for the rebuilding phase after the tsunami disaster, which destroyed many buildings in Phuket and Phang Nga. This phase started not earlier than March 2005, three months after the disaster and after the end of the emergency response and recovery phase.

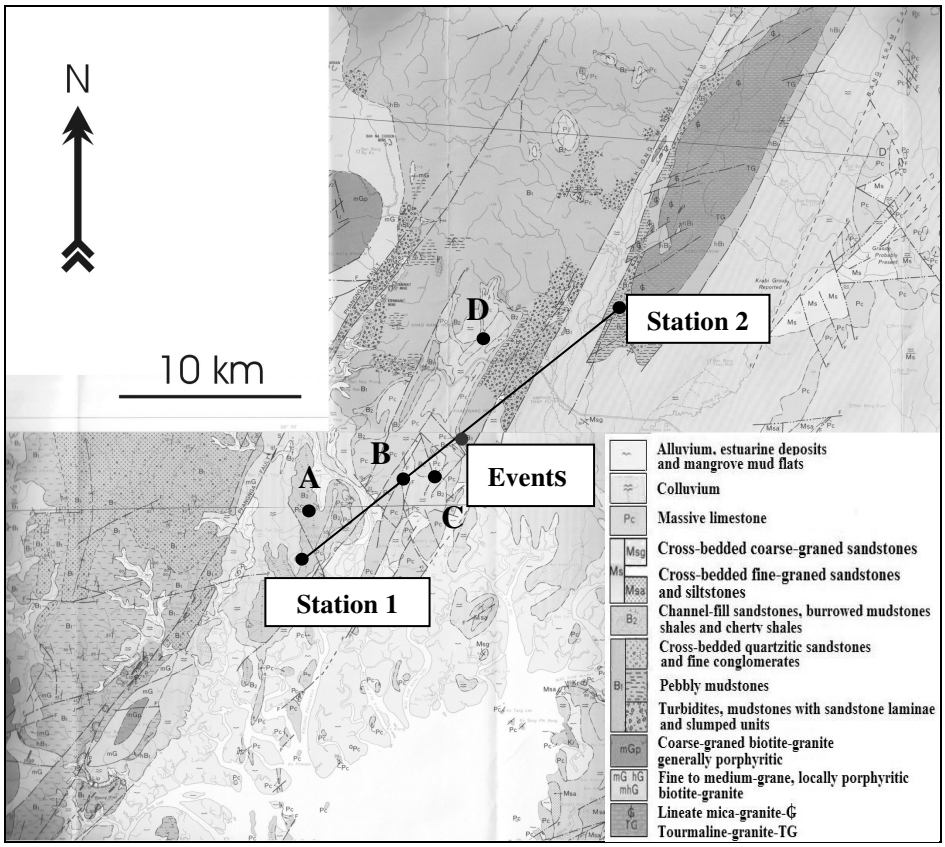

Figure 4.20. Geological map of Mueang District and Thap Put District, Phang Nga Province where the seismic station set up. A, B, C and D are limestone quarry locations. The average location of all man made seismic events is also shown (Garson and Mitchell, 1975).

4.5 Conclusions

The Mw 9.3 Sumatra-Andaman Earthquake on the 26 December 2004 with the subsequent tsunami had devastating effects on the Andaman coastlines of Thailand. Vertical movement of the ocean floor had triggered the tsunami. However, this major earthquake with the numerous aftershocks also resulted in significant horizontal movements of the Eurasian lithosphere to the West, recorded by GPS stations in Thailand, Malaysia and Indonesia.

As this study has shown, these horizontal movements of the lithosphere can be correlated with local earthquake activities in Southern Thailand, which were recorded by the PSU Short Period Seismic Network from 14 June to 30 June 2005.

In this period of nearly 6 months, 210 local seismic events were detected, 173 local earthquake events and 37 man made events. The local earthquakes occurred in an area between latitude 7.25 ˚N and 10.12 ˚N, and between longitude 97.26˚ E and 99.69˚ E, mainly on land, some in the Andaman Sea and one in the Gulf of Thailand. The man made events are likely from blasting activities in a limestone quarry, Quarry C, in Phang Nga Province at UTM, Zone 47, 453350 E, and 936440 N. The local magnitude values of all local events range between Ml -1.4 to Ml 2.2 following Hutton and Boore (1987). The local magnitudes of the man made events are all equal or below Ml 0.0. All the earthquake parameters, origin time, location and magnitude, are associated with uncertainties from numerous factors, like the chosen velocity model, depth considerations, or seismogram analysis with the identification of P- and S-wave arrival.

The distribution of the earthquake locations show that several earthquakes are aligned in nearly linear trends, which were interpreted as earthquake activities from fault movements. The main faults are the Khlong Marui Fault Zone in Phuket and Surat Thani Province and the Ranong Fault Zone further north, but also other faults seem to have been generated earthquakes. Nevertheless, several earthquake locations are not following obvious linear trends, they appear to be more cluster like in Phuket and Phang Nga Province.

The 26 December 2004 Earthquake unlocked the interface at the subduction zone between the Indian-Australian Plate in the west and the Eurasian Plate in the East. This resulted in the westwards movement of the Eurasian Plate. However, due to the pre-existence of the major fault zones in Southern Thailand differential movement was observed by several GPS stations on the Malaysian Peninsular. This is the result of the reactivation of these faults zones and the subsequent generation of the local earthquakes recorded by the PSU Seismic Network in Southern Thailand. Parallel to the movement, relaxation processes inside the Eurasian Plate also generated earthquakes, however not following linear trends, rather cluster like trends. All these earthquakes occurred in an extensional stress regime and therefore the lower magnitude values are reasonable. Additionally, the relaxation and extension resulted in an increased number of sinkhole occurrences in Southern Thailand.

Finally, this study has shown that the 26 December 2004 Earthquake had significant effects on Thailand. First, the earthquake triggered a massive tsunami that resulted in the death of more than 5,000 people in Thailand. Second, during and after the earthquake, the southern peninsula moved significantly to the west, 26 cm in about 8 minutes coseismically. This movement reactivated the faults zones in southern Thailand with subsequent earthquake occurrences.